Quantitative Determination of the Optimal Scale for the Proportion of Saline-Alkali Patches of Soda Saline-Alkali Land in Northeast China

Yakun Cao, Guanglei Hou, Ziqi Chen, Yanfei Gong, Jinyuan Zhou, and Zhaoli Liu

***Abstract*—As an important index reflecting the degree of soil salinization and alkalization, the proportion of saline-alkali patches (PSP) is beneficial for identifying the degree of saline-alkali land on a large scale with high spatial heterogeneity. However, determining the optimal scale for observing PSP remains inconclusive. In this article, we considered a typical area of saline-alkali land, which is located in Da'an City in Northeast China, as an example and selected nine sample areas from the sentinel-2A remote sensing images to calculate the salt index. According to the semivariogram function, we obtained the spatial autocorrelation range of the average radius of saline-alkali land. By combining the Nyquist-Shannon sampling theory, we determined the optimal scale for the remote sensing monitoring of saline-alkali land in Da'an City. The PSP index is calculated using this scale. The results were as follows: First, the optimal scale for the remote sensing monitoring of saline-alkali land in Da'an City is 41.2 m, and the calculated PSP index at this scale has the best correlation with the measured *pH* value data ($R^2 = 0.828$). Second, Using the PSP index calculated at this scale, we divided the degree of saline-alkali land in Da'an City into three grades. Among them, the slightly, moderately, and severely saline-alkali lands cover areas of 90.52, 111.78, and 959.77 km2, respectively. In this article, we propose a new method for grading the degree of soil salinization and alkalization on land with high spatial heterogeneity, providing technical support for the utilization of saline-alkali land.**

***Index Terms*—Grading and mapping, optimal scale, semivariogram function, soda saline-alkali land in Northeast China, the proportion of saline-alkali patches (PSP).**

Manuscript received 14 December 2023; revised 23 January 2024; accepted 9 February 2024. Date of publication 16 February 2024; date of current version 1 March 2024. This work was supported in part by the National Key Research Program under Grant 2021YFD1500104-3, in part by the Strategic Priority Research Program of the Chinese Academy of Sciences under Grant XDA28110503 and in part by Graduate Innovation Fund of Jilin University. *(Corresponding author: Zhaoli Liu.)*

Yakun Cao is with the Northeast Institute of Geography and Agroecology, Chinese Academy of Sciences, Changchun 130102, China, and also with the University of Chinese Academy of Sciences, Beijing 100049, China (e-mail: caoyakun21@mails.ucas.ac.cn).

Guanglei Hou and Zhaoli Liu are with the Northeast Institute of Geography and Agroecology, Chinese Academy of Sciences, Changchun 130102, China (e-mail: houguanglei@iga.ac.cn; liuzhaoli@iga.ac.cn).

Ziqi Chen is with the Jilin University, Changchun 130102, China (e-mail: chenzq0227@163.com).

Yanfei Gong is with the Changchun Institute of Engineering, Changchun 130102, China (e-mail: gongyanfei97@163.com).

Jinyuan Zhou is with the Jilin Agricultural University, Changchun 130102, China (e-mail: zjy516666@126.com).

Digital Object Identifier 10.1109/JSTARS.2024.3366773

I. Introduction

SALINE-ALKALI land, which is an important resource for agricultural development, is defined as saline-alkali grassland or saline-alkali bare land. Soda saline-alkali land is concentrated in Northeast China, with tremendous potential for development [1], [2], [3]. Conducting large-scale acquisition of information regarding the degree of land salinization and alkalization is crucial to optimizing land resource allocation, ensuring national food security, and promoting socio-economic development according to the local conditions [4], [5], [6].

In recent years, remote sensing technology has enabled the acquisition of large-scale information on saline-alkali land. Conventional statistical regression and intelligent machine learning methods are predominantly employed to assess the degree of land salinization and alkalization. By constructing a model that links soil spectral indices from remote sensing with measured soil point data, the degree of saline-alkali land can be obtained. Alternatively, the degree of land salinization and alkalization can indirectly be inferred from the inhibitory effects of soil salinity and alkalinity stress on vegetation [7]. However, owing to the high spatial heterogeneity of saline-alkali land in Northeast China, describing its variation characteristics at the spatial polygon-level solely based on measured point-level data is challenging. This approach has shortcomings, such as poor accuracy and high cost. To overcome these challenges, creating a polygon-level index that can directly characterize the degree of land salinization and alkalization is crucial. Considering the difficulties of relying solely on measured point-level data, this method enables a more accurate and cost-effective assessment of salinization and alkalization levels.

The national standard for the grading indicators of natural grassland degradation, desertification, and salinization issued in 2003 [8] states that the proportion of saline-alkali patches (PSP) is a polygon-level indicator reflecting the degree of saline-alkali land, which can be used to characterize the proportion of saline-alkali patch areas to grassland areas. The higher the PSP, the more severe is the degree of land salinization and alkalization. However, currently, this indicator is roughly estimated through manual visual inspection and has poor accuracy. Moreover, owing to the uneven size of saline-alkali patches in soda saline-alkali land, the PSPs obtained at different scales of remote sensing observation are not always the same, making them rarely applicable on a large scale.

As a hot issue, many scholars have carried out a lot of research on the optimal scale, which has been applied in urban landscape [9], [10], lake landscape [11], farmland landscape [12], and other directions. However, choice of the optimal scale is still an unsolved problem. During the remote sensing monitoring, if the observation scale is too large, the accuracy of the monitoring results is insufficient. On the contrary, if the observation scale is too small, more job and cost will be needed. The optimal observation scale can reveal the real distribution law of ground objects to the greatest extent [11]. Therefore, determining the observation scale to calculate PSP is a prerequisite for its application.

Previous studies have indicated that an appropriate observation scale for land features can be selected based on the range of spatial autocorrelation [11], [12]. The size of the range of spatial autocorrelation of the saline-alkali patches in the average state can help characterize the average size of the saline-alkali patches and can be used to determine the optimal scale of the observation. At this observation scale, we considered that the degree of spatial variation of saline-alkali patches inside the window is similar or the same (homogeneous units), making it a suitable observation unit for calculating the PSP.

The semivariogram function in geostatistics is a classical method to describe the spatial variation of ground objects and explore the spatial autocorrelation of landmarks [13], [14]. This can explain the spatial heterogeneity of land features caused by natural or human factors and quantitatively characterize spatial heterogeneity information. Wen et al. [12] investigated the heterogeneity of farmland landscapes in the Sanjiang Plain based on a semivariogram function, quantitatively analyzed the spatial heterogeneity of the target study area, and determined the optimal scale for remote sensing monitoring. Chen [15] established a spatial heterogeneity model for urban heat islands based on a semivariogram function and analyzed their spatial variation characteristics and spatial scale effects. Atkinson and Aplin [16] and Atkinson and Curran [17] used a semivariogram function to analyze the maximum correlation distance between observation samples and determine the optimal resolution in remote sensing applications.

In this article, the semivariogram function was used to determine the optimal scale of observations of saline-alkali patches in the study area, calculate the PSP, and quantitatively ascertain the variation characteristics and ranges of saline-alkali patches. Finally, the PSP was used as the grading index to classify the saline-alkali land in Da'an City.

II. Study Area and Data Collection and Pre-Processing

A. Study Area

The study area was Da'an City, Jilin Province, which is located in the Baicheng area of western Jilin Province. The wind period in this region is long, the spatial and temporal uniformity of precipitation is poor, and the degrees of land salinization and alkalization are significant. The main type is soda saline-alkali land [2], [5], which is highly representative of the processes of land salinization and alkalization in the Songnen Plain [17], [19].

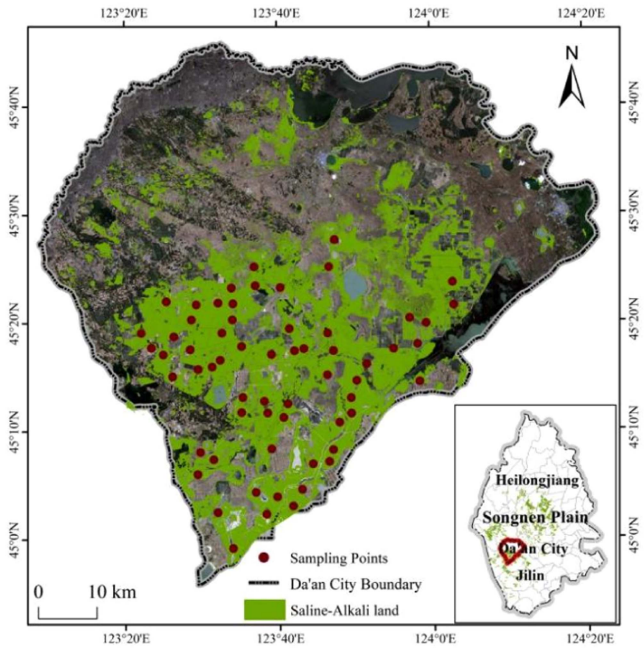

Fig. 1. Location of the study area in Songnen plain and sampling points distribution (note: The image in display is sentinel-2 data (R:G:B = band 4:3:2) and the green patches represent the range of saline-alkali land).

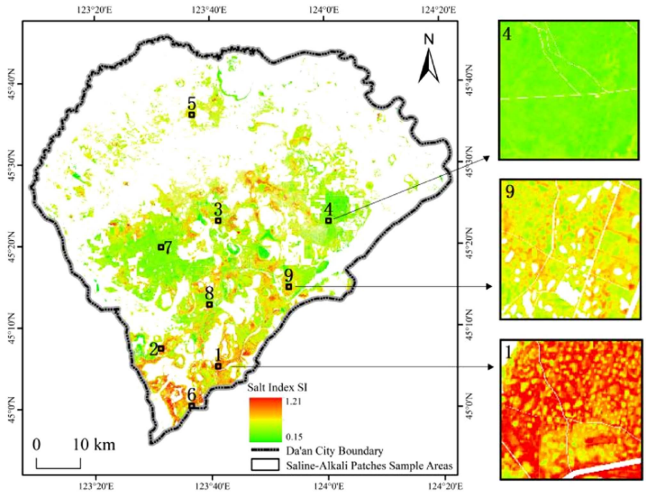

Fig. 2. Distribution of the typical sample areas.

The research object in this article was the saline-alkali land in Da'an City, namely, saline-alkali grassland and saline-alkali bare land. Using land-use data from 2020, the range of saline-alkali land in Da'an City was superimposed, as shown in Fig. 1. To better reflect the spatial heterogeneity characteristics of the entire study area, we used a 1500 × 1500-m grid to divide the salt index (SI) data in the study area into sample areas of equal sizes, as shown in Fig. 2. According to the equidistant method, the *SI* is layered into three levels (0.15–0.50: level 1; 0.50–0.86: level 2; and 0.86–1.21: level 3). The average SI values within each sample area were used to classify the values into different levels. Combined with the different spatial patterns of saline-alkali land, in each grade of random sampling, a total of 9 typical

sample areas were selected (three sample areas for each grade, of which sample areas 4, 5, and 7 were grade 1; sample areas 3, 8, and 9 were grade 2; and sample areas 1, 2, and 6 were grade 3). To the best of our knowledge, different types of ground-object-variation structures have been included to improve the representativeness.

B. Data Collection and Pre-Processing

1) Remote Sensing Image Data: We obtained 4 sentinel-2 level 2A surface reflectance images taken from June 2022 from the European Space Agency using the Google Earth Engine (GEE) platform (see Fig. 1).

On the one hand, because the rainy season in Northeast China is August and September, and June is not significantly affected by rainfall, alkali patches are more easily identified on the image. On the other hand, the fractional vegetation coverage is low, and the alkali patches have not been completely covered, which can distinguish saline-alkali land from bare soil.

These data included 13 spectral bands, namely, visible light, near-infrared, and shortwave infrared, as well as three quality assessment bands (i.e., quality assessment band). The spatial resolution of the image is 10 m. Cloud and shadow mask processing was conducted, and the cloud cover was less than 5%. Then, we mosaicked these Sentinel-2 remote sensing images by the same acquisition date and clipped them to the scope of the study area using GEE.

2) Actual Measured Soil Data: In this article, 62 topsoil samples (0–20 cm) were collected in the range of grassland and bare land in Da'an City in June 2022 (see Fig. 1). And each soil sample was collected at least 200 m off the road, and five sites were mixed as one soil samples. The samples were naturally dried, ground and sieved (1 and 0.25 mm). The soil pH was determined by soil suspension and pH meter (pHS-25) with a water-soil ratio of 5:1.

III. Methodology

Fig. 3 shows the flowchart. First, the SI value was calculated based on sentinel-2 images and then by binarizing the SI data, the saline-alkali and nonsaline-alkali patch data of Da'an City were obtained. Second, based on the semivariogram, the optimal observation scale of the PSP is determined, and the *PSP* is calculated on the binarized data. Finally, the degree of salinization and alkalization of land in Da'an City was obtained.

A. Equations of Spectral Index SI and Identification of Saline-Alkali Patches

The blue and red bands are highly sensitive to soil salinity [5], [21], [22], [23]. Therefore, the salt spectral index SI [(1), where B and R represent the blue and red bands, respectively] was applied in this article, and its binarized saline-alkali and nonsaline-alkali patch data were used as the basis for calculating the PSP

$$\mathrm{SI} = \sqrt{B \times R}. \tag{1}$$

On the basis of visual interpretation, first, 60 pure alkali patch pixels region of interest (ROI) were selected in the original sentinel image. Secondly, we identified a set T, which includes the minimum *SI* value (denoted as minx) in each ROI of saline-alkali patch pixels. Finally, we selected the smallest value t (2) from the set T as the threshold of image binarization processing. So, as to identify saline-alkali and non-saline-alkali patches

$$T = \left\{ \min_1, \min_2, \min_3 \ldots\ldots \min_n \right\}$$
$$t = \min(T). \tag{2}$$

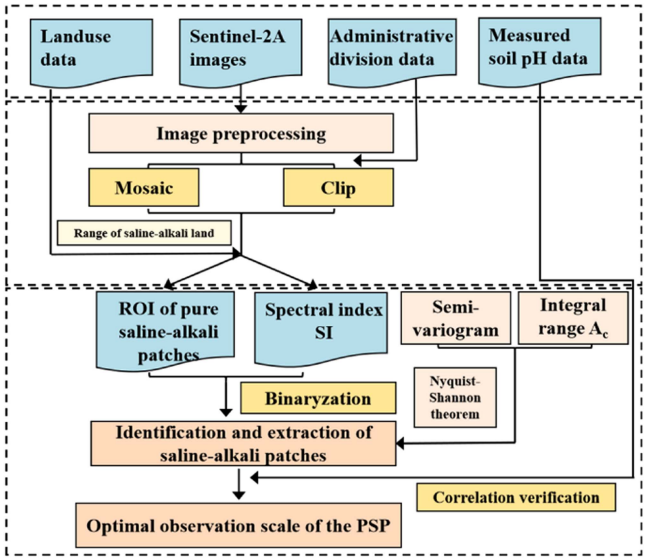

Fig. 3. Flowchart of this article.

B. Determination of the Range of Spatial Autocorrelation of Saline-Alkali Land

As a tool for spatial variation structure analysis, the semivariogram function is based on the second-order stationary hypothesis, which is the theoretical foundation of geostatistics. It is mainly used to analyze the overall spatial distribution characteristics of target attributes, distribution of structure, spatial randomness, and spatial autocorrelation [24], [25], [26], [27]. Based on the semivariogram function, the salinity index SI is used as a regionalized variable; namely, the SI value is a function of the spatial coordinate position of the pixel [26], [27]. Thus, it is used to describe the variation characteristics of saline-alkali land in the study area and quantitatively express the range of spatial autocorrelation of saline-alkali land in Da'an City.

1) Experimental Semivariogram Function: The SI values of any positions x and $x + h$ are denoted as $Z(x)$ and $Z(x + h)$, respectively. The vector distance between the two is h, and the number of point pairs in the image range that meet the conditions is $N(h)$. Half of the relative increment variance in the difference between the two was the semivariogram value. The calculation equation is expressed as follows:

$$\hat{\gamma}(h) = \frac{\sum_h [Z(x) - Z(x+h)]^2}{2N(h)}. \tag{3}$$

For the selection of the vector distance h in a certain direction (such as east-west or south-north), the maximum variation

TABLE I
DIFFERENT FITTING MODELS OF THE SEMIVARIOGRAM AND THEIR INTEGRAL RANGE EQUATIONS

Model	Formula	A_c
Exponential model	$\gamma(h)=\begin{cases}(C_0+C)^2\left(\frac{3}{2}\frac{h}{r}-\frac{1}{2}\left(\frac{h}{r}\right)^3\right), h\le r\\ (C_0+C)^2, h>r\end{cases}$	$\pi h^2/5$
Spherical model	$\gamma(h)=(C_0+C)^2\left(1-\exp\left(-\frac{3h}{r}\right)\right)$	$2\pi h^2/9$

distance of the calculated experimental semivariogram is 1/3 of the space range I of the image (1500 × 1500 m), namely, 500 m [12], [28]. It was 700 m in all directions. The maximum spacing of the *SI* values was selected without considering the direction. We used the professional software GS+ 7.0 to calculate the experimental semivariogram of the nine sample areas.

2) Theoretical Semivariogram Function: We aimed to reflect the spatial heterogeneity characteristics of the *SI* value in the entire distance and all directions, and quantitatively analyze the spatial variation characteristics of the *SI* value in different directions and distances. We used the correlation model (the fitting models used in this article were the spherical and exponential models) to fit the theoretical semivariogram function of the discrete values obtained by the experimental semivariogram function and obtain the relevant variation characteristic parameters. The equation is expressed as follows:

$$\gamma(h)=\frac{E[Z(x)-Z(x+h)]^2}{2}. \tag{4}$$

In (4), $\gamma(h)$ is the theoretical semivariogram value (hereinafter referred to as the semivariogram value). $Z(x)$ and $Z(x+h)$ represent the values of the regionalized variable *SI* at a distance $|h|$.

Theoretically, when the distance between two SI values is zero [24], the semivariogram value should also be zero. However, owing to the complexity of the actual geographical environment, the semivariogram value is greater than zero, which is called a nugget, representing the random variation of the SI value. When $\gamma(h)$ reaches a certain value, it tends to be stable and no longer increases.

At this point, the semivariogram value is called the sill [29], [30], and the transition from nugget to sill is called the partial sill. The sill represents the overall spatial variability of the *SI* value, including random factors and structural spatial variations. The degree of variation in the SI that is affected by the spatial structure can be determined from a partial sill. The nugget-to-sill ratio (nugget-sill ratio) is used to quantify the proportion of random variations [11], [13]. h is the step distance corresponding to the first time of sill realization, which is called the effective range A. The range represents the maximum distance of spatial autocorrelation between *SI* sample values. When this value is exceeded, the spatial correlation is significantly weakened or even irrelevant.

3) Determination of the Range of Spatial Autocorrelation Under the Average State: Owing to complex changes in the actual geographical environment, the quantitative characterization of multiscale and multi-level spatial heterostructures is still weak. Therefore, an index integral range A_c was used in this article, which organically integrates the spatial structure (spatial autocorrelation) and spatial variability [28], [31] to quantitatively express the spatial heterogeneity. The integral range A_c is expressed as follows:

$$A_c=\frac{1}{(C_0+C)^2}\int\left((C_0+C)^2-\gamma(h)\right)dh. \tag{5}$$

In (5), $\gamma(h)$ is the semivariogram fitting model selected in the sample area, and the integral range equations corresponding to the exponential and spherical models are given in Table I.

The arithmetic square root D_c is used to express all the structural parameters of the fitted model into a single feature distance, which is the weighted average of the parameters in different spatial ranges. It was used to characterize the spatial autocorrelation range of the average state of the *SI* images in the study area. It can be used as a standard to determine whether the spatial scale of an image is sufficiently large to detect alkali spot information [26].

4) Calculation of the PSP: We developed a coarsening algorithm program based on Python [32], setting the window on the image and side length as the optimal observation scale. Considering the example of a saline-alkali patch pixel, as shown in Fig. 4, the 2 × 2 window comprises four layers, and all the pixels in the four-layer window of the upper left, lower left, upper right, and lower right are used. The average value was accumulated and the coarsening result was used as the new pixel value for the image. The sliding window is used to calculate the PSP of the entire image [33].

5) Accuracy Assessment: The Pearson correlation coefficient is used to measure whether the two datasets are on a

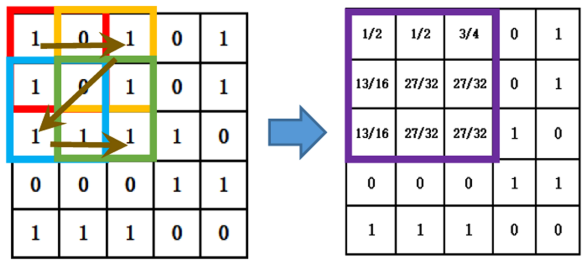

Fig. 4. Schematic diagram of the coarsening algorithm.

TABLE II
NATIONAL GRADING STANDARDS FOR THE DEGREE OF LAND SALINIZATION AND ALKALINIZATION

Rate of saline-alkali patches (%)	*pH*	Degree of land salinization and alkalization
≤15%	8.5–9	Slight
15%—30%	9–9.5	Moderate
30%—50%	9.5–10	Severe
≥50%	>10	Extremely severe

line, which can reflect the linear relationship between the fixed distance variables [34]. The calculation equation is expressed in (6): we estimated the observation scale of the saline-alkali patches according to the different settings and calculated the PSP. Pearson's bivariate correlation analysis was conducted using the SPSS software to analyze the correlation between the PSP value and measured pH sample point values. The rationality and accuracy of the scale were verified, and the optimal scale showed the highest correlation

$$P = \frac{N\sum x_i y_i - \sum x_i y_i}{\sqrt{N\sum x_i^2 - (\sum x_i)^2}\sqrt{N\sum y_i^2 - (\sum y_i)^2}}. \quad (6)$$

In the (6), P represents the Pearson correlation coefficient, N represents the amount of data of independent variables, and x and y represent two independent variables, respectively.

6) Classification Standard of Saline-Alkali Land: According to the national classification standard for the salinization and alkalization of PSP index (GB-19377-2003) [8], we classified and mapped the degree of land salinization and alkalization in the study area. The standard is as Table II.

IV. RESULTS

A. Types of GraphicsResults of Extraction of Saline-Alkali Patches

The threshold for the extraction of saline-alkali patches in the study area was set to 0.24 (2), and the SI image was binarized. The recognition results are shown in Fig. 5. The number of saline-alkali patch pixels was 1.35 x 10^7, accounting for 64% of the total number of pixels. The number of nonalkali spot pixels was 7.68 x 10^6, accounting for 36% of the total number. Combined with the land-use dataset of 2020, the pixels of saline-alkali patches were randomly selected, and the kappa coefficient was used for the consisten-cy test. When $K = 0.70$, the classification results were highly consistent, and the accuracy was good.

B. Determination of the Optimal Scale of PSP Observation

1) Omnidirectional Spatial Heterogeneity Analysis: In this article, the normality of the nine sample areas was tested. The results showed that the data for the remaining seven sample areas deviated from the normal distribution, except for sample areas 6 and 9. Therefore, standardized preprocessing must be conducted, such as standard normal, square root, and logarithmic transformations, on SI data. Semivariogram fitting

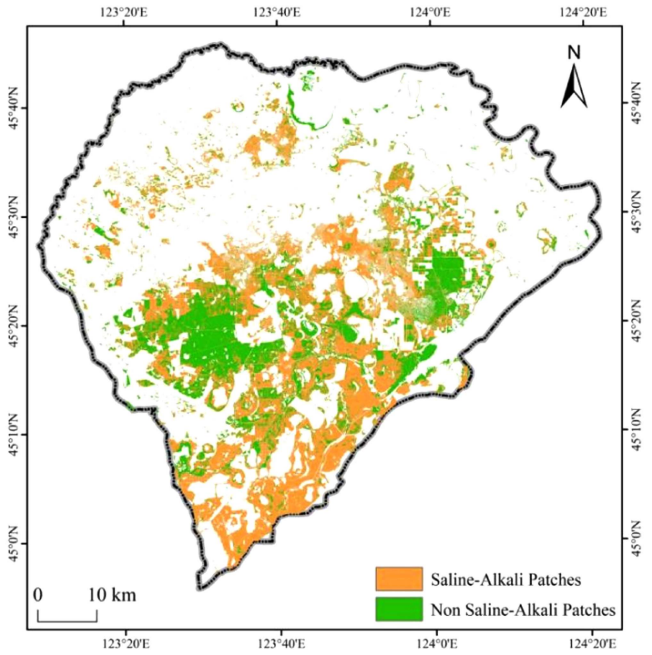

Fig. 5. Results of the identification of saline-alkali patches.

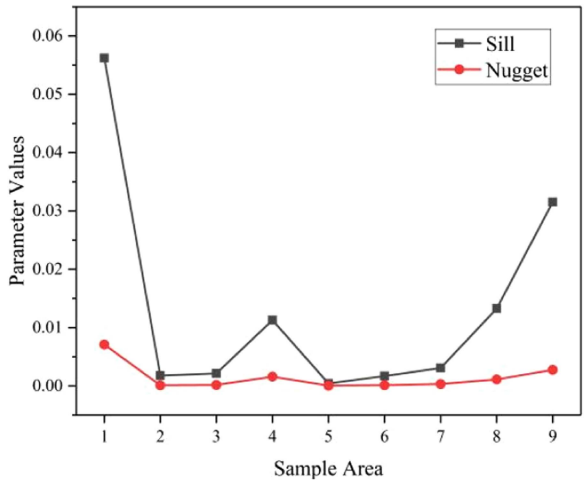

Fig. 6. Changes in fitting parameters of various zones.

of SI data was conducted using different models to obtain the corresponding fitting parameters, as given in Table III.

Based on the two parameters of fitting accuracy, namely, R^2 and fitting variance root mean square error (RMSE), we determined the optimal fitting model and its fitting parameters for each sample area. As given in Table III, except for sample area 6, the optimal fitting results for the other sample areas were exponential, and the optimal fitting of sample area 6 was spherical. The sill value of sample 1 was the highest, indicating that sample 1 had the largest spatial variation (see Figs. 6 and 7), strongest structure, and was the most easily identifiable. The sill value of sample area 5 was the smallest, indicating that the overall spatial variation of this sample area was the smallest and the structure was the weakest. Combined with remote sensing images, we can determine whether landscapes of different types

TABLE III
OMNIDIRECTIONAL VARIOGRAM FITTING INFORMATION OF THE NINE SAMPLE AREAS

	Transformation method	Model	Nugget	Sill	*A* (range)	Nugget-sill ratio	RSS	R^2
Area 1	*N*	S	0.000600	0.055400	59.00	0.011	1.711×10^{-4}	0.600
	Z-score	E	0.007100	0.056200	102.00	0.126	1.130×10^{-4}	0.745
Area 2	*N*	S	0.000004	0.001728	67.00	0.002	2.153×10^{-7}	0.642
	Sqrt-Root	E	0.000113	0.001766	123.00	0.064	1.046×10^{-7}	0.838
Area 3		S	0.000001	0.002122	66.00	0.001	1.497×10^{-7}	0.785
	Sqrt-Root	E	0.000179	0.002148	108.00	0.083	6.150×10^{-8}	0.914
Area 4	*n*	S	0.000500	0.011100	64.00	0.045	6.664×10^{-6}	0.633
	Log	E	0.001590	0.011280	120.00	0.141	3.012×10^{-6}	0.850
Area 5	*N*	S	0.000016	0.000424	55.00	0.038	3.446×10^{-9}	0.750
	Sqrt-Root	E	0.000051	0.000427	81.00	0.119	1.729×10^{-9}	0.881
Area 6	*Y*	S	0.000131	0.001702	102.00	0.077	2.742×10^{-8}	0.968
		E	0.000247	0.001714	135.00	0.144	2.761×10^{-8}	0.965
Area 7	**N**	S	0.000882	0.003054	105.00	0.289	2.093×10^{-7}	0.873
	Log	E	0.000333	0.003076	114.00	0.108	1.724×10^{-7}	0.895
Area 8	**N**	S	0.000060	0.012920	67.00	0.005	1.819×10^{-5}	0.548
	Log	E	0.001130	0.013260	126.00	0.085	1.237×10^{-5}	0.702
Area 9	**Y**	S	0.000800	0.031500	48.00	0.061	1.245×10^{-5}	0.691
		E	0.002760	0.031520	54.00	0.025	1.225×10^{-5}	0.696

Remark：1) N is non-normal and Y is normal.
2) Z-score: standard normal transform; Sqrt-root: square root transform; log: log transform.
3) S: Spherical model; E: Exponential model.

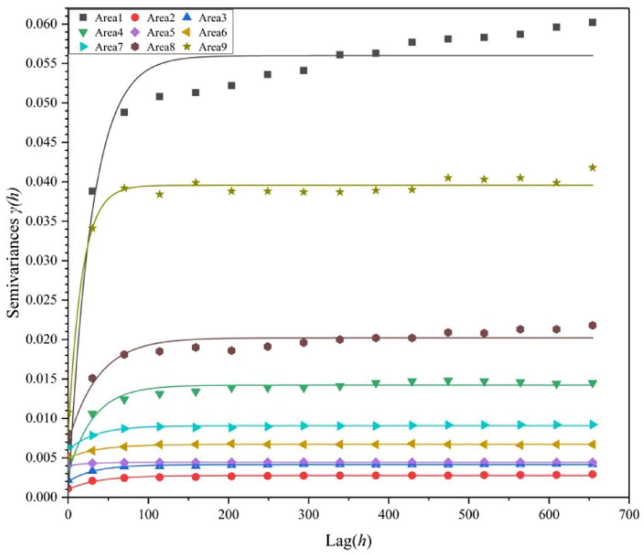

Fig. 7. Schematic diagram of the optimal fitting range values for each sample area.

of ground objects have large spatial heterogeneity. When the saline-alkali patches are concentrated and other ground objects are evenly interspersed in a small amount, or when no other ground objects are present, the spatial variability is small. Moreover, we found that the nugget value is generally low, the nugget-sill ratio is not more than 10%, and the overall nugget effect is not obvious. Therefore, the influence of random factors on the spatial heterogeneity of saline-alkali patches was ignored in this article.

TABLE IV
OMNIDIRECTIONAL VARIOGRAM FITTING INFORMATION FOR THE NINE RESEARCH POINTS

Sample Area	Optimal fitting *A* (m)	A_c (m)	D_c (m)
1	102	6537.03	80.85
2	123	9505.83	97.50
3	108	7328.71	85.61
4	120	9047.79	95.12
5	81	4122.40	64.21
6	102	7263.36	85.23
7	114	8165.63	90.36
8	126	9975.18	99.88
9	54	1832.18	42.80

2) Determination of the Optimal Observation Scale: According to the optimal fitting range value of each sample area, the A_c value and its square root $D_c(x)(x = 1,2,3,\ldots,9)$ were calculated, as given in Table IV Combined with the Nyquist-Shannon sampling theorem, when the remote sensing observation scale is less than $D_c/2$, the spatial autocorrelation range in the average state of the saline-alkali patches can be detected and the spatial heterogeneity of the saline-alkali patches can be distinguished. Within the sample area of this observation scale, we considered that the degree of saline-alkali land is the same. The optimal scale of PSP observation was set to $D_c/2$ in the article.

3) Verification of the Optimal Observation Scale: The D_c value was set differently according to the maximum value of 99.88 m, minimum value of 42.8 m, and average value of 82.4 m in each sample area $D_c(x)$. For the three $D_c(x)$ values, the correlation between the PSP value and measured pH value was

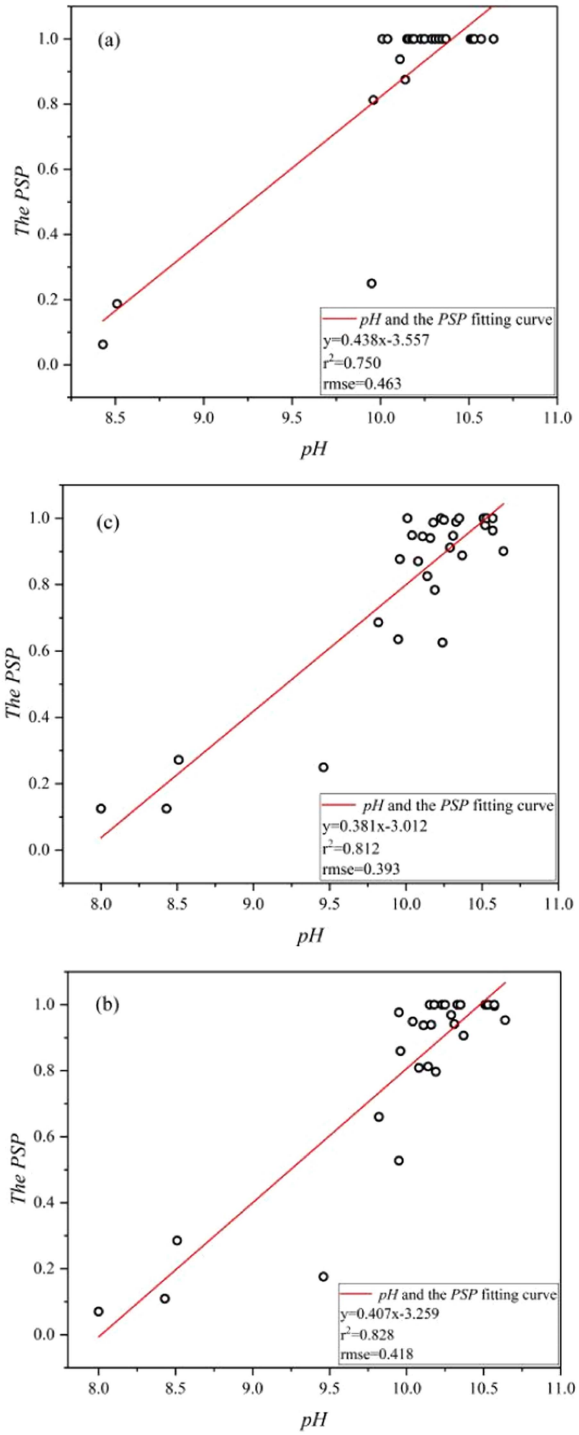

Fig. 8. Linear model of pH to the PSP where Dc is the minimum value (a), average (b), maximum value (c).

analyzed, and a linear fitting model was established to verify the rationality of the scale. A positive correlation was observed in all three cases ($P < 0.05$).

When the minimum value of D_c of 42.8 m was considered, the observation scale is $D_c/2 = 21.4$ m, and the accuracy of the linear fitting model between the PSP and measured pH value was 0.75 and the RMSE was 0.463, as shown in Fig. 8(a). When the average value of D_c of 82.4 m was considered, the observation scale was $D_c/2 = 41.2$ m, and the accuracy of the linear fitting model between the PSP and measured pH value (R^2) was 0.828 and the RMSE was 0.418, as shown in Fig. 8(b). When the maximum value of D_c of 99.88 m was considered and the observation scale was $D_c/2 = 49.94$ m, the accuracy R^2 of the linear fitting model between the PSP and measured pH value was 0.812 and the RMSE was 0.393, as shown in Fig. 8(c).

Under the observation scales obtained using the three different D_c values, the positive correlation between the PSP and measured pH value does not imply that the larger the observation window, the higher is the correlation between the above two variables. In this article, the scale with the highest correlation (namely, the average D_c was 82.4 m, and the observation scale was $D_c/2 = 41.2$ m) is the final optimal observation scale.

TABLE V
AREA AND PROPORTION OF EACH DEGREE OF LAND SALINIZATION AND ALKALIZATION

Degree of land salinization and alkalization	Area (km^2)	Ratio
Non	350.84	23.19%
Slight	90.52	5.98%
Moderate	111.78	7.39%
Severe	959.77	63.44%

C. Classification Mapping of Saline-Alkali Land

The above sections showed that the optimal scale of PSP observations in the study area was 41.20 m. Based on this scale, an observation window was set to calculate the PSP in the study area, and the saline-alkali land in Da'an City was graded. The total area of saline-alkali land in Da'an City is 1162.07 km^2, among which the area of slightly saline-alkali land is 90.52 km^2, accounting for 5.98% of the total area of saline-alkali land. The area of moderately saline-alkali land is 111.78 km^2, accounting for 7.39% of the total area of saline-alkali land. The area of severely saline-alkali land is 959.77 km^2, accounting for 63.44% of the total area of saline-alkali land (see Table V and Fig. 9).

V. DISCUSSION

A. Implication of the PSP

The study generates saline-alkali and nonsaline-alkali patch data by binarizing *SI* data, and then calculates the PSP on this basis. We have obtained some spectral indices commonly used in other studies, combined with the index pH that can show the degree of salinization and alkalization of land. Then, we compared and analyzed the correlation between these indices and the measured pH value of the soil, and selected the spectral indices according to the strength of the correlation. As shown in the Fig. 10., the correlation between SI and the measured pH value is the best, which can better reflect the salinization and alkalization of land. Therefore, we adopted SI as the spectral index to carry out research.

Notably, PSP refers to the proportion of the saline-alkali patch area to the window area in the unit observation window, as shown in Fig. 11, which is a polygon-level index that can be

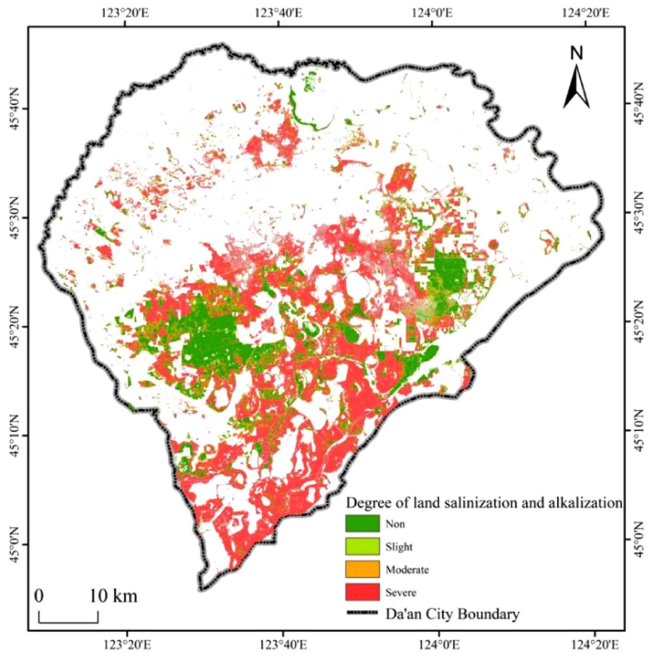

Fig. 9. Classification map of the degree of land salinization and alkalization in Da'an city.

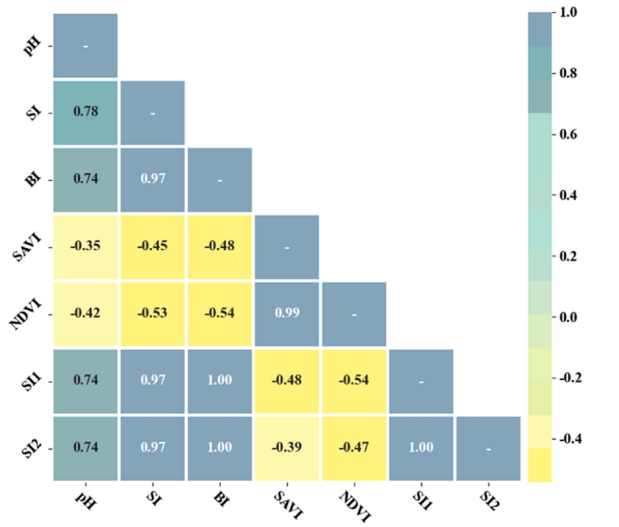

Fig. 10. Heat map of the correlation between these indices and the measured pH value of the soil.

directly obtained from the remote sensing spectrum. This can overcome the deviation between the inversion results of the nonlinear model and real values of the traditional remote sensing inversion method for pixels with spatial heterogeneity.

In 1986, Liu and He [35] created a map of soil salinization in the Xisongnen Plain and reported that the area affected by soil salinization in this area was 1.23×10^4 km^2, whereas the estimated area of soil salinization studied by Yu et al. [36] was considerably lower than the previously estimated area. The results of Yu et al. [36] showed that from 1991 to 2016, the increase in the area of farmland covered by salt in the western

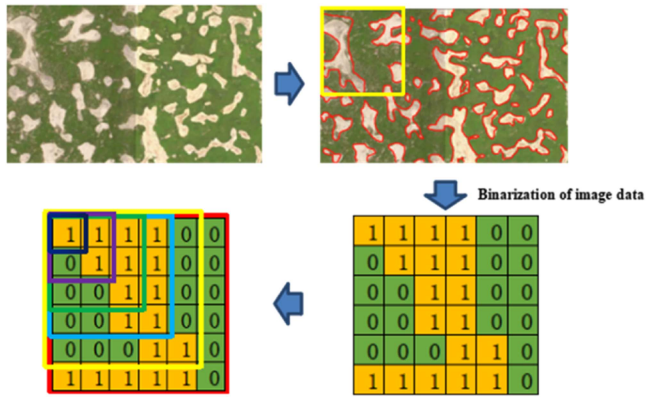

Fig. 11. Schematic diagram of the PSP principle.

plain of Songnen was the main contributor (59.13%) to the salt-affected area expansion, whereas those of Li et al. [5] and other studies suggested that 25% of saline soil was converted into farmland; thus, the two results were different. The above study was based on *EC* point data. Compared with this method, that based on the area index *PSP* can more accurately reflect the real change characteristics of ground objects. It can effectively reduce the error caused by the internal difference between mixed pixels, overcome the difficulty of a single point in representing the spatial polygon-scale features of pixels, and describe the degree of land salinization and alkalization in land with high spatial heterogeneity. The key problem in applying the PSP is the optimal observation window scale.

Wen et al. [12] quantitatively expressed spatial heterogeneity through a semivariogram function, and introduced a method of using the integral range A_c combined with the Nyquist sampling theorem to select the optimal scale. However, this method lacks the necessary verification steps for practical applications. We not only determined the optimal observation scale from a theoretical perspective but also verified it on the basis of measured data, and applied it to practice.

B. Anisotropic Heterogeneity Analysis

The spatial variability function values of the three different grades of typical SI sample areas were extracted and calculated from the south-north (0°), northeast-southwest (45°), east-west (90°), and northwest-southeast (135°) directions (see Fig. 12; sample areas 1, 4, and 9).

In the south-north direction [see Fig. 12(a)], an obvious inflection point was observed between sample areas 4 and 9 at an interval of approximately 80 m, indicating that the two sample areas have clear spatial structures in this space. Combined with Fig. 2, we inferred that this structure is a road inside the saline-alkali land. Subsequently, the experimental semivariogram curves changed smoothly and no other obvious inflection points appeared. The semivariogram value of the inflection point accounted for a large proportion of the maximum value in the entire semivariogram curve. This indicates that in these two sample areas, the spatial structure characteristics comprising roads are significant in this direction, which is the

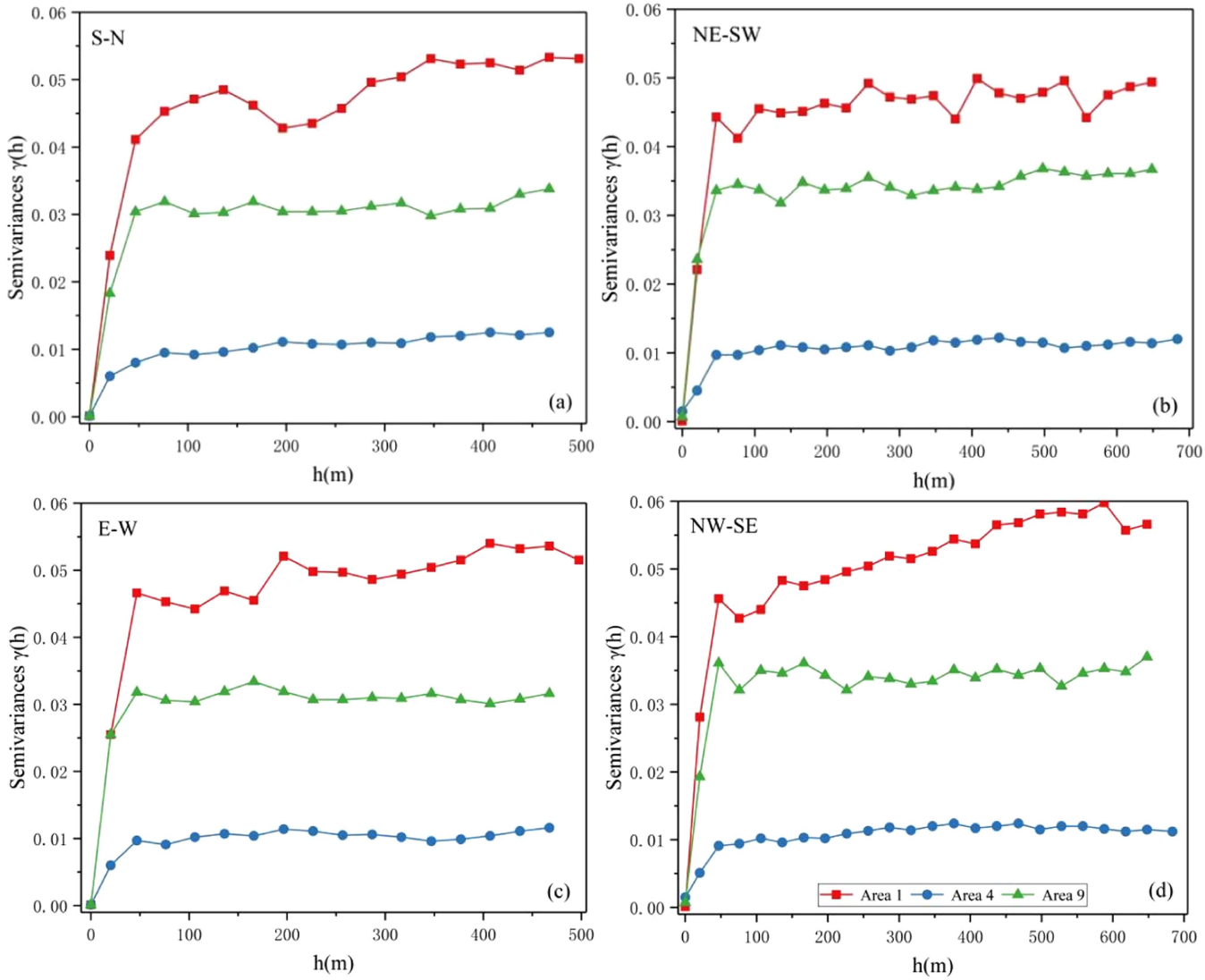

Fig. 12. Experimental semivariogram values of the three grades of typical sample areas in the north-south direction (a), northeast-southwest direction (b), east-west direction (c), northwest-southeast direction (d).

main cause of spatial heterogeneity. The semivariogram curve of sample area 1 fluctuated the most. We observed an obvious variation peak at an interval of approximately 150 m, a trough at 200 m, and a maximum at 350 m, reflecting the spatial structure characteristics caused by different sizes of saline-alkali patches.

In the east-west direction [see Fig. 12(c)], obvious inflection points were observed in the three sample areas at intervals of approximately 50 m, indicating that the spatial variability can be detected at this scale. However, the trend of the variation curve in the east-west direction of sample area 1 was opposite to that in the south-north direction, and the maximum variation was observed at 200 m. This indicated that the spatial structure characteristics in the east-west direction of the spatial structure characteristics in the east-west direction of the sample area were not similar to those in the south-north direction.

The longitudinal comparative observation in Fig. 12 shows that the variation values of sample areas 1 and 4 were the largest and smallest, respectively, which was determined by the spatial structure of the saline-alkali patches and grassland in the sample area. However, similarities were observed between the variogram curves for each sample area. For example, the change curves of sample area 4 in the four directions were similar; however, the first wave peak in the south-north direction was slightly backward, the grassland was widely distributed, and almost no saline-alkali patch distribution was observed, indicating the lack of significant difference in spatial heterogeneity in the four directions of sample area 4. In sample area 9, except for the northwest-southeast direction, the other three directions show similar curve changes, indicating that the spatial variation direction of sample area 9 is northwest-southeast, which is attributed to the distribution of saline-alkali patches of different sizes in this direction. Sample area 1 shows the most complex situation, but as indicated by the observed variation values, the variation value is the highest in the northwest-southeast direction, which is caused by the mosaic arrangement of roads and saline-alkali patches.

Through the structural analysis of the experimental semivariogram function, combined with the anisotropy of the study area, the size and direction of spatial heterogeneity in the area can be fully understood. In addition, the natural and man-made driving factors can be identified to supplement the theoretical basis for determining the optimal observation window scale of PSP.

C. Analysis of the Spatial Distribution Characteristics of Land Salinization and Alkalization

The degree of land salinization and alkalization in Da'an City is mainly severe, and most areas are distributed in the central and southern parts of Da'an City. Saline-alkali land is concentrated and contiguous, especially in the southern region.

Notably, the salinization and alkalization of high-coverage grassland in Da'an City are more serious, which is consistent with the results of Zhang and Li [37]. Wu et al. [16] concluded that the area of severe saline-alkali land in Da'an City accounted for 60.33% of the total area of saline-alkali land. We found that the proportion of severe saline-alkali land in Da'an City was 63.44%, which is similar to the results of the aforementioned previous study. The mildly saline-alkali land is mainly located on the east and west sides of the middle of the city, which may be owing to the control measures in Da'an City in recent years to combat land salinization and alkalization, such as planting saline-alkali-resistant vegetation, rice planting, and raising fish. These measures have caused the recession of farmland in the central region and increase in the number of ponds, which can ensure timely river water supply; thus, the degree of land salinization and alkalization is low.

D. Inovations and Limitations of Our Study

The perspective in this article is different from the previous remote sensing inversion and spatial expansion that based on the measured soil point data. Instead, the polygon-level indicator index PSP is used as an indicator to reflect the degree of salinization and alkalization of land, which can overcome the point-level indicator errors caused by the high spatial heterogeneity of soda saline-alkali land in Northeast China. The goal of this article is the calculation of the PSP. Previously, the PSP was mostly roughly estimated by artificial vision, lack of quantitative method.

In this article, it is different from the previous application to determine the spatial resolution of remote sensing satellite monitoring. The semivariogram combined with the integral range was used to estimate the observation scale of the PSP, in order to calculate the PSP scientifically and quantitatively. So, that it can be closest to the real change law of the saline-alkali land in the study area, and carry out more accurate monitoring.

By observing the linear correlation between the PSP and pH, we found that PSP had a good response in high-pH areas. However, whether the PSP is more suitable for highly saline-alkaline land still needs to be ascertained. Simultaneously, during the quantitative analysis of spatial heterogeneity in the study area and the determination of the optimal observation scale, the number of typical sample areas can be appropriately increased to cover more types of landscape patterns, or other statistical parameters, such as variance and standard deviation, can be used to integrate different observation scales in each sample area to ensure the feasibility of studying the degree of salinization and alkalization of land on a large scale.

VI. Conclusion

In this article, SI data were obtained based on sentinel-2A images, and the saline-alkali patches in the range of saline-alkali land in Da'an City were identified. Based on the theory of geostatistical semivariograms, the integral range ac was introduced to integrate the range of spatial autocorrelation and spatial variation. Its square root D_c was used to determine the range of spatial autocorrelation of saline-alkali land in Da'an City under the average state of saline-alkali patches. Combined with the Nyquist-Shannon sampling theorem, the optimal scale of saline-alkali patches observations in the study area was determined. The correlation between the measured soil pH and PSP was analyzed using the Pearson bivariate correlation analysis method, and the rationality of the observation scale was verified. The classification and mapping of saline-alkali land in Da'an City were realized according to the existing national classification standard for saline-alkali land using *PSP*. The main conclusions are as follows.

1) The SI data were constructed based on the blue and red bands of sentinel-2A data. Through binary segmentation, the saline-alkali patches in the range of saline-alkali land in Da'an City could be identified. The kappa coefficient was used for the consistency test, namely, $K = 0.70$, the classification results were highly consistent and the accuracy was good.
2) Landscapes with the same type of ground objects have low heterogeneity, but they vary with the influence of small-scale spatial variation (such as roads and canals). A landscape with a mosaic distribution of different types of ground objects has great spatial heterogeneity, but shows great differences with different mosaic distribution modes. A landscape with a scattered distribution mode has clear spatial structural characteristics, and its total spatial variability is large. The clustered mosaic landscape had spatial structural characteristics at different scales, and the spatial variation was relatively small.
3) Based on the geostatistical semivariogram theory, combined with the Nyquist–Shannon sampling theorem, our analysis showed that the optimal scale for the observation of PSP in Da'an saline-alkali land was 41.20 m. The *PSP* calculated at the optimal scale showed good correlation with the measured soil pH values. The linear correlation (R^2) between the two was 0.828, and the RMSE was 0.418.
4) Considering PSP as the index, the limitations of remote sensing inversion monitoring and classification mapping of large-scale saline-alkali land based on point-level data were overcome. Combined with the national classification standard for saline-alkali land, the classification of saline-alkali land in Da'an City was realized. This shows that severely saline-alkali land was prominent in Da'an City, accounting for 63.44% of the total, and the area of slightly saline-alkali land is relatively small. Land salinization and alkalization in Da'an City are serious issues and require urgent treatment.

ACKNOWLEDGMENT

The authors greatly appreciate the anonymous reviewers and editors, and thank the European Space Agency for sharing the sentinel 2 remote sensing images.

REFERENCES

[1] B. Wu et al., "A nondestructive conductivity estimating method for saline-alkali land based on ground penetrating radar," *IEEE Trans. Geosci. Remote Sens.*, vol. 58, no. 4, pp. 2605–2614, Apr. 2020, doi: 10.1109/TGRS.2019.2952719.

[2] L. Xiaoyan, W. Zongming, and Z. Shuwen, "Dynamic analysis and prediction of saline-alkali land in the western part of Northeast China," in *Proc. IEEE Int. Geosci. Remote Sens. Symp.*, 2005, pp. 1886–1890.

[3] X. Yang and Y. Yu, "Estimating soil salinity under various moisture conditions: An experimental study," *IEEE Trans. Geosci. Remote Sens.*, vol. 55, no. 5, pp. 2525–2533, May 2017, doi: 10.1109/TGRS.2016.2646420.

[4] S. W. Zhang, J. C. Yang, Y. Li, Y. Z. Zhang, and L. P. Chang, "Changes of saline-alkali land in Northeast China and its causes since the mid-1950s," *J. Natural Resour.*, vol. 25, no. 3, pp. 435–442, 2010.

[5] X. Li, Y. Li, B. Wang, Y. Sun, G. Cui, and Z. Liang, "Analysis of spatial-temporal variation of the saline-sodic soil in the west of Jilin Province from 1989 to 2019 and influencing factors," *Catena*, vol. 217, 2022, Art. no. 106492.

[6] H. Jiang, Y. S. F. J. RuSuli, J. Kadir, and A. Wufu, "Evaluation and analysis of soil salinization in arid oasis based on neural network model," *Geo-Inf. Sci.*, vol. 19, no. 7, pp. 983–993, 2017.

[7] J. Wang, X. N. Liu, F. Huang, J. L. Tang, and L. B. Zhao, "Salinity forecasting of saline soil based on ANN and hyperspectral remote sensing," *Trans. Chin. Soc. Agricultural Eng.*, vol. 25, no. 12, pp. 161–166, 2009.

[8] "The grading index of natural grassland degradation, desertification and salinization of the Ministry of Agriculture of the People 's Republic of China," 2003.

[9] D. Han et al., "The roles of surrounding 2D/3D landscapes in park cooling effect: Analysis from extreme hot and normal weather perspectives," *Building Environ.*, vol. 231, 2023, Art. no. 110053, doi: 10.1016/j.buildenv.2023.110053.

[10] D. Han et al., "How do 2D/3D urban landscapes impact diurnal land surface temperature: Insights from block scale and machine learning algorithms," *Sustain. Cities Soc.*, vol. 99, 2023, Art. no. 104933, doi: 10.1016/j.scs.2023.104933.

[11] J. Chen, B. J. Wang, J. Fu, and X. J. Gao, "Using moving window approach to estimate the intrinsic scale of the circulation of suspended sediment movement in Taihu Lake," *J. Hydroecol.*, vol. 32, no. 5, pp. 1–5, 2011, doi: 10.15928/j.1674-3075.2011.05.006.

[12] Z. F. Wen, S. Q. Zhang, J. Bai, C. H. Ding, and C. Zhang, "Agricultural landscape spatial heterogeneity analysis and optimal scale selection: An example applied to sanjiang plain," *Acta Geographica Sinica*, vol. 67, no. 3, pp. 346–356, 2012, doi: 10.11821/xb201203006.

[13] H. B. LiQ, Z. Wang, and Q. C. Wang, "The theory and method of quantitative research on spatial heterogeneity," *Chin. J. Appl. Ecol.*, no. 6, pp. 93–99, 1998, doi: 10.3321/j.issn:1001-9332.1998.06.018.

[14] S. Garrigues, D. Allard, F. Baret, and J. Morisette, "Multivariate quantification of landscape spatial heterogeneity using variogram models," *Remote Sens. Environ.*, vol. 112, no. 1, pp. 216–230, 2008, doi: 10.1016/j.rse.2007.04.017.

[15] Z. Chen, "Spatial variation in land cover and choice of spatial resolution for remote sensing," M.S. thesis, Dept. Comput. Technol., Chongqing Posts Telecommun. Univ., Chongqing, China, 2019.

[16] P. M. Atkinson and P. Aplin, "Spatial variation in land cover and choice of spatial resolution for remote sensing," *Int. J. Remote Sens.*, vol. 25, no. 18, pp. 3687–3702, 2004, doi: 10.1080/01431160310001654383.

[17] P. M. Atkinson and P. J. Curran, "Defining an optimal size of support for remote sensing investigations," *IEEE Trans. Geosci. Remote Sens.*, vol. 33, no. 3, pp. 768–776, May 1995, doi: 10.1109/36.387592.

[18] H. S. Wu and Z. L. Liu, "Remote sensing and mapping of saline sodic land based on spectral characteristics for Da'an City," *Soils Crops*, no. 2, pp. 178–182, 2007, doi: 10.3969/j.issn.1001-0068.2007.02.013.

[19] S. L. Liu, Y. H. Dong, N. N. An, J. Wang, and H. D. Zhao, "Saline-alkaline land dynamics in the Songnen Plain based on enhanced vegetation index series and landscape pattern analysis–A case study of Daan City," *Chin. J. Appl. Ecol.*, vol. 25, no. 11, pp. 3263–3269, 2014, doi: 10.13287/j.1001-9332.20140918.017.

[20] Y. H. Dong, S. L. Liu, N. N. An, Y. J. Yin, J. Wang, and Y. Qiu, "Landscape pattern in Da'an City of Jilin Province based on landscape indices and local spatial autocorrelation analysis," *J. Natural Resour.*, vol. 30, no. 11, pp. 1860–1871, 2015, doi: 10.11849/zrzyxb.2015.11.007.

[21] X. Wang, Y. H. Li, R. Y. Wang, F. Z. Shi, and S. T. Xu, "Remote sensing inversion of organic matter content in winter wheat surface soil at nodulation stage based on unmanned aerial vehicle," *Chin. J. Appl. Ecol.*, vol. 31, no. 7, pp. 2399–2406, 2020, doi: 10.13287/j.1001-9332.202007.023.

[22] Y. H. Dai, Y. Guan, C. Y. Feng, M. Jiang, and X. H. He, "Extraction and analysis of soil salinization information of Alar reclamation area based on spectral index modeling," *Remote Sens. Natural Resour.*, vol. 35, no. 1, pp. 205–212, 2023, doi: 10.6046/zrzyyg.2021427.

[23] R. S. Dwivedi and B. Rao, "The selection of the best possible landsat TM band combination for delineating salt-affected soils," *Int. J. Remote Sens.*, vol. 13, no. 11, pp. 2051–2058, 1992, doi: 10.1080/01431169208904252.

[24] X. W. Li, C. X. Cao, and C. Y. Chang, "The first law of geography and spatial-temporal proximity," *Nature*, vol. 29, no. 2, pp. 69–71, 2007, doi: 10.3969/j.issn.0253-9608.2007.02.002.

[25] A. F. Rahman, J. A. Gamon, D. A. Sims, and M. Schmidts, "Optimum pixel size for hyperspectral studies of ecosystem function in southern California chaparral and grassland," *Remote Sens. Environ.*, vol. 84, no. 2, pp. 192–207, 2003, doi: 10.1016/S0034-4257(02)00107-4.

[26] P. Han and J. Y. Gong, "A review on cholce of optimal scale in remote sensing," *Remote Sens. Inf.*, vol. 1, pp. 96–99, 2008, doi: 10.3969/j.issn.1000-3177.2008.01.019.

[27] S. Garrigues, D. Allard, F. Baret, and M. Weiss, "Quantifying spatial heterogeneity at the landscape scale using variogram models," *Remote Sens. Environ.*, vol. 103, no. 1, pp. 81–96, 2006, doi: 10.1016/j.rse.2006.03.013.

[28] R. D. Zhang, *The Theory and Application of Spatial Variation*. Beijing, China: Sci. Press, 2005, pp. 83–87.

[29] C. E. Woodcock, A. H. Strahler, and D. L. Jupp, "The use of variograms in remote sensing: I. Scene models and simulated images," *Remote Sens. Environ.*, vol. 25, no. 3, pp. 323–348, 1988, doi: 10.1016/0034-4257(88)90108-3.

[30] R. Webster, "Quantitative spatial analysis of soil in the field," in *Proc. Adv. Soil Sci.*, 1985, vol. 3, pp. 1–70.

[31] C. Lantuéjoul, "*Geostatistical Simulation: Models and Algorithms*. Berlin, Gernmany: Springer, 2001, pp. 503–513.

[32] J. Serra, "*Image Analysis and Mathematical Morphology*. Cambridge, MA, USA: Academic, 1982, pp. 96–97.

[33] H. Zheng, "Research on the mechanism of remote sensing image spatial pattern detection by comparing local variance and variation function methods," Ph.D. dissertation, Dept. IGA., Chin. Acad Sci. Univ., Beijing, China, 2014.

[34] P. Zang, "Remote sensing classification mapping of saline alkali wasteland grasslands in western Jilin," M.S. thesis, Dept. Geo-Exploration Sci. Technol., Jilin Univ., Jilin, China, 2023.

[35] Z. M. Liu and Y. He, "Research on land saline-alkalized in the west of Jilin province," *Resour. Sci.*, vol. 26, no. 5, pp. 111–116, 2004, doi: 10.3321/j.issn:1007-7588.2004.05.016.

[36] H. Yu, Z. Wang, D. Mao, M. Jia, S. Chang, and X. Li, "Spatiotemporal variations of soil salinization in China's West Songnen Plain," *Land Degradation Develop.*, vol. 34, no. 8, pp. 2366–2378, 2023, doi: 10.1002/ldr.4613.

[37] Q. Zhang and M. Y. Li, "Analysis of dynamic changes of saline-alkali land in Da 'an City based on GIS and remote sensing," *Geol. Spatial Info Technol.*, vol. 42, no. 10, pp. 65–68, 2019, doi: 10.3969/j.issn.1672-5867.2019.10.019.

Yakun Cao is currently working toward the graduate degree in cartography and geographic information system with the Northeast Institute of Geography and Agroecology, Chinese Academy of Sciences, Changchun, China and also belongs to the University of Chinese Academy of Sciences, Beijing, China.

Her research direction is ecological remote sensing of saline-alkali land, observation scale, and remote sensing inversion of saline-alkali land.

Guanglei Hou received the Ph.D. degree in cartography and geographic information system from Northeast Normal University, Changchun, China, in 2012.

Since 2012, he has been a Senior Engineer of the project with the Northeast Institute of Geography and Agricultural Ecology, Chinese Academy of Sciences. He has presided more than ten scientific research projects, such as the National Natural Science Foundation of China, the National Key Research and Development Projects, and the National Key Fund Projects. He has authored or coauthored more than 20 academic papers, participated in one monograph, authorized 4 patents, and 8 software copyrights. His main research direction is ecosystem remote sensing.

Ziqi Chen is currently working toward the Ph.D. degree in geomatics engineering with the School of Jilin University, Changchun, China.

Her research direction is ecosystem and assessment.

Yanfei Gong is currently working toward the master's degree in geomatics engineering with Changchun Institute of Engineering, Changchun, China.

His research direction is the evaluation and improvement of saline-alkali land, and the development of model promotion system.

Jinyuan Zhou is currently working toward the graduate degree in agricultural engineering and information technology with Jilin Agricultural University, Changchun, China.

His research direction is the research on the demarcation of the threshold of land salinization degree.

Zhaoli Liu received the Ph.D. degree in remote sensing and geographic information system from the Institute of Remote Sensing Applications, Chinese Academy of Sciences, Beijing, China, in 2001.

He is currently a Researcher of the Northeast Institute of Geography and Agricultural Ecology, Chinese Academy of Sciences, Beijing, China. Over the years, he has presided over and participated in a number of national and provincial scientific research projects, authored or coauthored more than 30 academic papers in Chinese and English in international and domestic, and authorized 3 invention patents. His research direction is the scale theory and technology application in ecological remote sensing, including remote sensing information and remote sensing model scale conversion.